

pubs.acs.org/acsapm Article

Magnetoactive Thermoplastic Elastomers with Bottlebrush Strands: Switching and Programming of Mechanical Properties by a Magnetic Field

Sergei A. Kostrov, Mitchell R. Maw, Sergei S. Sheiko,* and Elena Yu. Kramarenko*



ACCESS

Cite This: ACS Appl. Polym. Mater. 2023, 5, 7458–7466

Metrics & More



Article Recommendations

 $T \uparrow$ $T \downarrow$ $T \downarrow$

ABSTRACT: We report on a distinct class of magnetoactive thermoplastic elastomers (MATEs) based on A-g-B bottlebrush graft copolymers filled with magnetic carbonyl iron microparticles. The A-g-B copolymers form a solvent-free elastomeric matrix providing tissue-mimetic softness and strain-stiffening, along with the capability of molding above a specific flow temperature. In contrast to covalently cross-linked magnetoactive elastomers, the mechanical properties and magnetic response of MATEs can be altered through particle rearrangement in a magnetic field at enhanced temperatures. This thermo-magnetic processing transforms the MATE from an isotropic to anisotropic composite with near three-fold increase in elastic modulus, up to 25% decrease in the damping factor, and up to 7.5-fold enhancement of the magnetorheological effect. The ability to reprogram the shape and viscoelasticity of MATEs has vital implications for the future of biomedical devices and soft robotics.

KEYWORDS: magnetoactive elastomers, magnetorheological effect, mechanical properties, damping factor, bottlebrush copolymers

■ INTRODUCTION

Magnetoactive elastomers (MAEs) are an important class of materials that are vital in devices such as peristaltic systems, artificial muscles, and other biomedical devices. These composite materials are generally composed of an elastic matrix as a passive medium loaded with ferromagnetic particles (MPs) to make the material "active" under an applied magnetic field. Rearrangement of the MPs due to magnetic interactions induced by a magnetic field results in altered physical properties (viscoelastic, magnetic, electric, and surface). The magnitude of the magnetic effect depends on the elastic modulus of the polymer matrix as well as the magnetic properties, concentration, and distribution of the MPs. For the magnetic properties, concentration, and distribution of the MPs.

Fundamentally, the mechanical properties of the matrix for a strong response should exhibit extreme softness of $E_0 \approx 1{\text -}10$ kPa, which is inaccessible for dry elastomer matrices due to intrinsic chain entanglements setting a lower boundary on modulus of ${\sim}10^5$ Pa. Overcoming this limitation currently relies on the addition of various diluents that may leach and thereby impact the mechanical integrity, strength, and long-term stability of the material. Additionally, anisotropic distribution of MPs in the matrix largely alters the magnetic response of the MAE, which is vital for soft robotics controlled

by an external magnetic field. 15,16,25,26 Though anisotropy can be attained by carrying out polymerization and cross-linking the matrix in a magnetic field, 17-24 the MPs are trapped in their cured state. MAEs cured with an isotropic distribution of particles may exhibit re-alignment of the particles in a magnetic field but revert back to an isotropic state when the field is removed. Neither of these procedures enable post-polymerization rearrangement of MPs within the polymer matrix.

Supporting Information

Herein, we present an advanced platform for the design of magnetoactive thermoplastic elastomers (MATEs) that possess a unique combination of (i) tissue-mimetic softness for magnetic response, (ii) strain-stiffening for strength, (iii) solvent-free molding for MATE fabrication, and (iv) structural reconfiguration to re-program properties on demand. At room temperature (RT), A-g-B bottlebrush graft copolymers form thermoplastic elastomers where chemically distinct block

Received: June 20, 2023 Accepted: August 4, 2023 Published: August 24, 2023





Figure 1. (a) A MATE based on an A-g-B brush-like copolymer networks with embedded magnetic microparticles at RT. Note that the mesh size (\sim 100 nm) is much smaller than the particle size (\sim μ m). (b) Reversible melting of the MATE at enhanced temperatures. (c) Altering properties of the MATE by structuring MPs in melt and quenching the melt in a magnetic field.

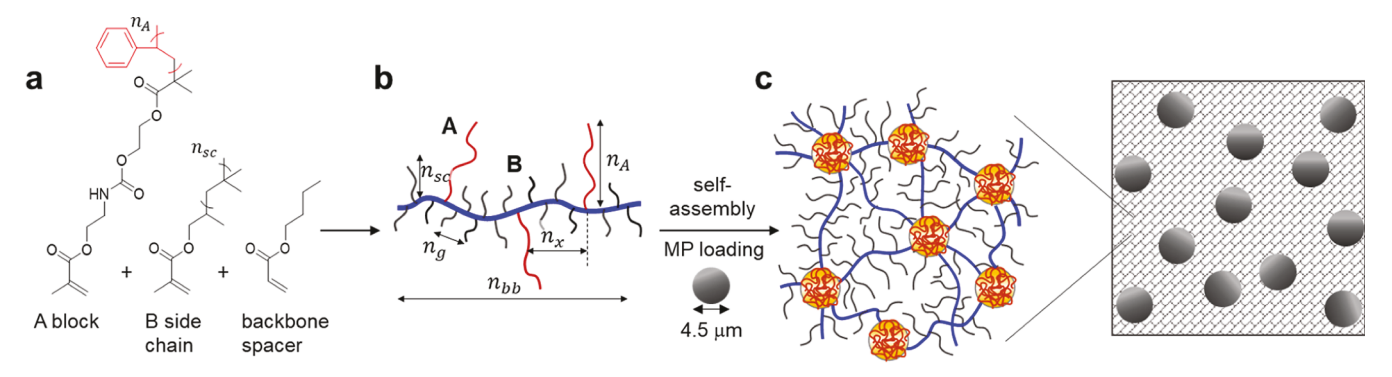


Figure 2. Preparation of MATEs. (a) Copolymerization of macromonomer yields (b) A-g-B brush-like copolymers with a controlled fraction of PS side chains (A block, $n_A = 60$) grafted onto a bottlebrush with PIB side chains (B block, $n_{sc} = 18$) and PBA spacers ($n_g = 8$). (c) Loading an A-g-B formulation with MPs followed by A-g-B self-assembly into a polymer network results in MATE.

microphases separate into network nodes interconnected by brush strands (Figure 1a).²⁷ Given the μ m-sized particles, the brush-like matrix is considered as a continuous medium, where viscoelastic properties are controlled by the A-g-B architectural parameters due to magneto-mechanical coupling being introduced on a micron scale.²⁸ Side chains tethered to the network strand dilute the network backbone to reduce entanglements enabling softness down to Young's modulus (E_0) of 10^3 Pa.²⁷ Upon application of a magnetic field to, the MATEs exhibit a reversible, on-demand increase in stiffness due to magnetization and alignment of the particles as chemically cross-linked MAEs do. Due to the softness of the A-g-B elastomeric matrix, a high level of magnetic response can be achieved in MATE without the addition of any diluent. Furthermore, in contrast to "passive" covalently cross-linked polymer matrices, the A-g-B network is thermally "active" as it melts at moderate temperatures (50-100 °C) (Figure 1b). This enables both molding of desired shapes as well as reconfiguration of the particles in a magnetic field followed by cooling back to RT to fix the shape and trap the particles in an anisotropic state (Figure 1c). With this platform, we instill a combination of magnetic and thermal control of MATE structures and properties in situ through combined magnetic field-temperature coordinates.

■ RESULTS AND DISCUSSION

Synthesis. Viscoelasticity of A-g-B systems is controlled by a set of distinct architectural parameters including the sidechain degree of polymerization (DP) $n_{\rm sc}$, DP between side chains $n_{\rm g}$, DP between A-blocks $n_{\rm x}$, total DP of the brush-like strand $n_{\rm bb}$, as well as DP and volume fraction of A-block $n_{\rm A}$ and $\phi_{\rm A}$, respectively (Figure 2a). PS-g-PIB brush-like graft copolymers were prepared by free-radical co-polymerization of pre-synthesized A-block and B-block macromonomers

(Supporting Information).²⁷ The polystyrene (PS) macromonomer (A-block) was synthesized by atom transfer radical polymerization of styrene to $n_A = 60$ followed by methacrylate functionalization through iso-cyanate chemistry (Scheme S1). Polyisobutylene (PIB) B-block macromonomers (n_{sc} = 18) were synthesized via two-step anti-Markovnikov bromine addition and subsequent methacrylate substitution from commercial methylvinylidene-functionalized PIB oligomer.^{29,30} The prepared A-block macromonomers, B-block macromonomers, and *n*-butyl acrylate spacers (Figure 2a) were copolymerized overnight ($n_g = 8$) and washed to remove any unreacted macromonomers, revealing the A-g-B brush polymer matrix (Figure 2b). The n_x of the copolymers was calculated by 1 H NMR, while GPC was utilized to estimate the $n_{\rm bb}$ by comparing the number average molecular weight M_n of the polymer to the molecular weight of a strand repeat unit (Figures S1 and S2). The $n_{\rm bb}$ was regulated by the initiator concentration in FR polymerization, but greater control may be achieved by controlled radical polymerization methods.² Note $n_{\rm bb}$ is vital for strength enhancement.

Preparation of Magnetic Composites. The MATEs were prepared by mixing A-g-B graft copolymers with a particular volume fraction of MPs (Figure 2c). Spherical MPs of 4.5 μ m diameter magnetically soft carbonyl iron (CI) (grade R-20, OOO SINTES-PKG) with coercivity equal to 9 \pm 3 Oe and specific magnetization equal to 190 \pm 8 emu/g were used in this study. A portion of the A-g-B brush copolymer was redissolved in 5× volume of dichloromethane with subsequent addition of the calculated volume fraction of MPs (ρ = 7.8 g/mL) and vigorously mixed. The solution was flash evaporated in a glass Petri dish lined with the Teflon film at 150 °C to prevent sedimentation of the MPs. The resultant MATE had an aerated structure where bubbles formed upon evaporation of dichloromethane. To remove the bubbles in the network,

Table 1. Mechanical Properties of A-g-B Brush-like MATEs

sample	$\phi_{ ext{MP}}{}^a$	$\phi_{\scriptscriptstyle m A}^{\;m b}$	n_x^c	$n_{\rm bb}^{d}$	$E (kPa)^e$	$G_{\rm e}~({\rm kPa})^f$	β^{g}	$E_0 (kPa)^h$	λ_{\max}^{i}	$\sigma_{ m max}~({ m kPa})^j$
2.5-0	0	0.025	969	1445	3.2	2.10	0.02	9.65	8.3	132
2.5-CI-5	5	0.025	969	1445	4.7	1.71	0.03	10.0	7.4	104
2.5-CI-10	10	0.025	969	1445	5.0	3.31	0.09	15.5	5.0	82
2.5-CI-20	20	0.025	969	1445	7.0	3.80	0.12	19.8	4.2	54
5-0	0	0.05	380	1394	21.7	9.15	0.07	51.3	5.4	320
5-CI-5	5	0.05	380	1394	25.9	6.25	0.09	48.0	3.9	260
5-CI-10	10	0.05	380	1394	36.9	1.05	0.11	51.7	3.3	220
5-CI-20	20	0.05	380	1394	43.8		0.23	63.5	2.1	100

"Volume fraction of MP with density $\rho = 7.8$ g/mL. "Volume fraction of A-block in the A-g-B brush copolymer matrix: $\rho_{PS} = 1.02$ g/mL, $\rho_{PIB} = 0.84$ g/mL, and $\rho_{PBA} = 1.08$ g/mL. "CDP of the network strand between A-blocks." DP of the A-g-B backbone. "Structural tensile modulus $E \approx k_b T \rho_s \frac{\langle R_{in}^2 \rangle}{s \, b_b R_{max}}$, where k_b is the Boltzmann constant, ρ_s is the density of stress-supporting strands, and b_k is the Kuhn length of stress supporting strands. Fortion of modulus due to entanglements. Strain-stiffening parameter. Young's modulus (eq 2). Elongation-at-break.

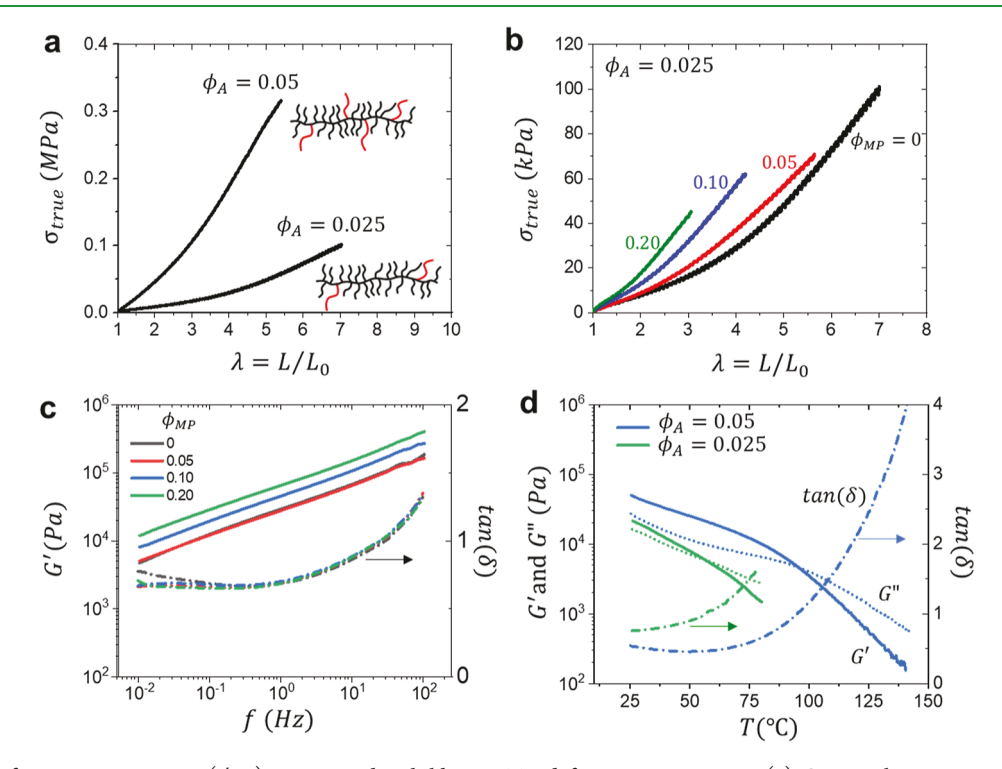


Figure 3. Effect of MP concentration (ϕ_{MP}) on A-g-B brush-like MATE deformation response. (a) Stress—elongation curves of neat A-g-B elastomers with different volume fractions of PS blocks. (b) Stress—elongation curves of A-g-B brush-like MATEs ($\phi_{\text{A}} = 0.025$ and $n_x = 969$) with different volume fractions of MPs as indicated. (c) Frequency sweeps of the A-g-B brush-like MATE series with $\phi_{\text{A}} = 0.025$ and $n_x = 969$. (d) Temperature sweeps of A-g-B brush-like copolymer matrices at a frequency of 1 Hz demonstrate network disassembly upon heating. The elastomer-to-melt transition temperature (T_{flow}) increases with ϕ_{A} .

the sample was hot-melt pressed at 100 °C into a thin homogeneous film with thickness ~1 mm. Two series of MATEs were prepared with different volume fractions of Ablock ($\phi_{\rm A}=0.05$ and 0.025) and corresponding $n_{\rm x}$'s at a constant $n_{\rm A}=60$. For each matrix, MP volume fractions ($\phi_{\rm MP}$) of 0.05, 0.10, and 0.20 were loaded (Table 1).

Mechanical Properties of A-*g*-**B Brush MATEs.** Neat A-*g*-B networks (without MPs) demonstrate the characteristic non-linear response to deformation observed for semi-flexible strands such as bottlebrush elastomers and collagen scaffolds in biological tissues (Figure 3a). Young's modulus E_0 and strain-stiffening parameter β , were determined by fitting the stress—elongation curves to the equation of state which describes true stress σ_{true} as a function of the elongation ratio, $\lambda = L/L_0$ from the initial length L_0 to instantaneous deformed length L as 36

$$\sigma_{\text{true}}(\lambda) = (\lambda^2 - \lambda^{-1}) \left(\frac{G_{\text{e}}}{\lambda} + \frac{E}{9} \right)$$

$$\left(1 + 2 \left(1 - \frac{\beta(\lambda^2 + 2\lambda^{-1})}{3} \right)^{-2} \right)$$
(1)

where $G_{\rm e}$ is the entanglement shear modulus, E is the structural modulus, and $\beta = \langle R_{\rm in}^2 \rangle / R_{\rm max}^2$ corresponds to extensibility of network strands relative to their contour length $R_{\rm max}$. The E, β , and $G_{\rm e}$ outputs yield Young's modulus as

$$E_0 = \frac{E}{3} \left(1 + \frac{9G_e}{E} + 2(1 - \beta)^{-2} \right)$$
 (2)

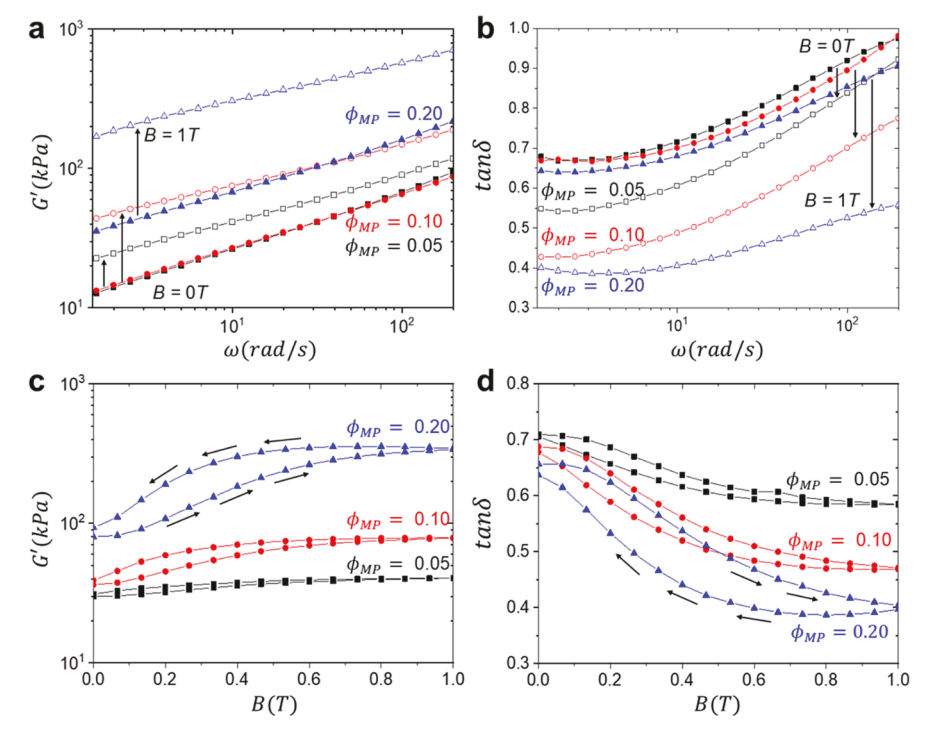


Figure 4. Effect of the magnetic field on viscoelastic properties of MATEs ($\phi_A = 0.025$) with different volume fractions of MPs (ϕ_{MP}) as indicated. Frequency dependence of (a) storage modulus and (b) tan δ of MATEs with different Fe concentrations measured at B = 0 and B = 1 T. Dependence of (c) storage modulus and (d) tan δ on magnetic flux density measured at $\omega = 10$ rad/s.

Table 2. MR Effect of A-g-B Brush-like MATEs

	MR effect in initial	isotropic samples at RT	induced ani	sotropy (5/1)	MR effect in produced anisotropic samples (4/5)		
sample	$\frac{\Delta G'}{G'_0}$, % ^a	$\frac{\Delta \tan \delta}{\tan \delta (B=0)}$, %	$\frac{G'(5)}{G'_0(1)}$ b	$\frac{\tan \delta(5) \mathbf{b}}{\tan \delta(1)}$	$\frac{\Delta G'}{G'_0}$, %	$\frac{\Delta \tan \delta}{\tan \delta (B=0)}, \%^{c}$	
2.5-CI-5	35	-18	1.81	1.02	210	-52	
2.5-CI-10	115	-32	1.62	0.87	856	-63	
2.5-CI-20	322	-39	2.88	0.75	798	-77	
5-CI-5	15	- 7	1.74	0.94	56	-25	
5-CI-10	97	-18	1.82	0.98	213	-43	
5-CI-20	154	-25	2.83	0.76	592	-64	

 a MR effect in the initial isotropic samples. b Induced anisotropy. c The MR effect in anisotropic samples produced after treatment with T_{max} = 98 $^\circ$ C. The 5/1 and 4/5 legends indicate the modulus ratios corresponding to states 1, 4, and 5 in Figure 5a.

obtained from the derivative of eq 1 at $\lambda \to 1$. All mechanical properties are summarized in Table 1 and correspond to a strain rate of $\dot{\epsilon}=0.005~\rm s^{-1}$. At small deformations, the A-g-B thermoplastic elastomers are relatively soft with $E_0\sim 10~\rm kPa$, which is on par with soft tissues such as skeletal muscle. The modulus of brush networks exhibits an exponential increase with deformation due to the proximity of the pre-extended backbones to full extention. The proximity of the pre-extended backbones to full extention. The proximity of the pre-extended backbones to full extention. The proximity of the pre-extended backbones to full extention.

Loading the A-g-B thermoplastic elastomers with MPs resulted in additional enhancement of strain-stiffening (Figure 3b and Table 1). With MP addition, each series ($\phi_{\rm A}=0.025$ and $\phi_{\rm A}=0.05$) exhibits nearly a 4–5× increase in firmness reaching $\beta\cong0.23$, which significantly exceeds $\beta\cong0.01$ of the conventional linear networks. It is important to note that despite $\phi_{\rm MP}$ increase up to 0.20, the brush MATEs remain soft comparable to vein and artery tissue ($E_0<20$ kPa for $\phi_{\rm A}=0.025$ and $E_0<65$ kPa for $\phi_{\rm A}=0.05$). ^{39,40} Trends in modulus are further verified by oscillatory frequency sweeps.

Mechanical properties of of the PS-g-PIB MATEs are strain rate and temperature dependent. Unlike linear networks trapped above the entanglement plateau ($G_{\rm e,lin} \sim 10^5$ Pa), the storage modulus of the architecturally disentangled brush MATEs decreases below the entanglement and remains time dependent through the frequency range of 10^{-2} and 10^2 Hz (Figure 3c). Minimal change in the damping factor ($\tan \delta$) is observed upon loading of the MPs. Given the physical nature of cross-links, both matrices undergo disassembly at moderate temperatures $T_{\rm flow}$ from 50 to 100 °C (Figure 3d). The ability to dis- and re-assemble MATEs using the A-g-B brush-like copolymer matrix is vital for material processing and programming the magnetic response as discussed below.

Magnetic Response of MATEs at RT. Application of a magnetic field considerably changed the viscoelastic properties of the MATEs. Figure 4a,b shows frequency dependence of the storage modulus and the damping factor, respectively, for the samples with a matrix of $\phi_A = 0.025$ with different fractions of MPs measured at magnetic field B = 0 T and B = 1 T. At a constant frequency, the MATEs exhibit a pronounced

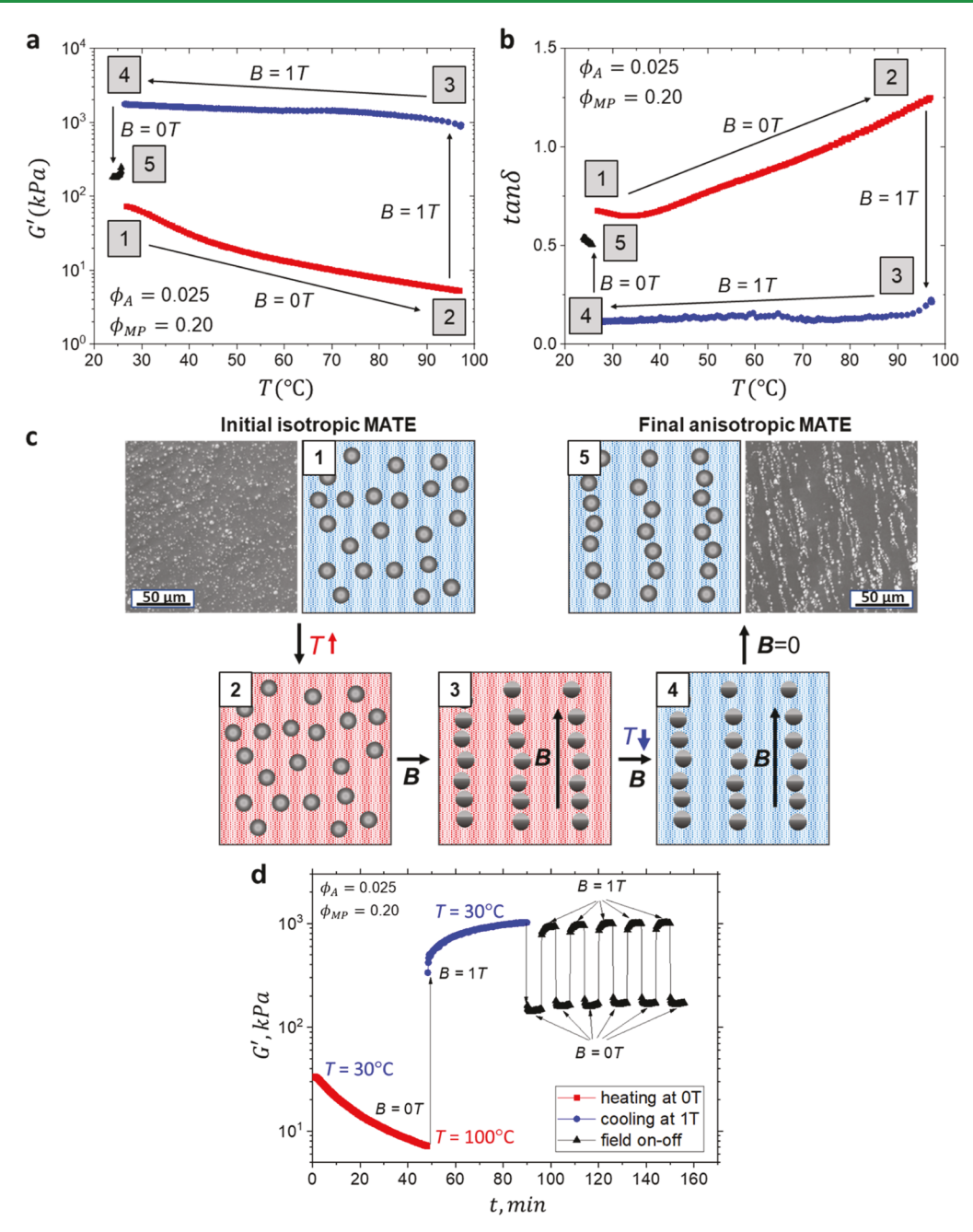


Figure 5. Creation of anisotropic magnetic structures by MATE annealing followed by cooling in a magnetic field. Temperature dependence of (a) storage modulus and (b) tan δ where arrows show the direction of temperature and magnetic field change: heating is performed at B=0 T magnetic field while cooling is carried out at B=1 T. (c) Schematic representation of various stages of sample heating and cooling in the magnetic field: 1—initial isotropic MATE at RT, 2—initial isotropic MATE heated to 98 °C, 3—aligned magnetic chains formed in melted MATE under the action of magnetic field, 4—magnetic chains fixed by the magnetic field in the course of MATE cooling back to RT, 5—final anisotropic MATE after turning off the magnetic field and annealing for 1 month at RT. SEM images of the MATE are inset for stage 1 and 5 showing MP rearrangement. (d) Time scan of the MATE processing according to (a) followed by a series of the on—off field alterations demonstrating a prompt and stable operation of the MATE with the newly programmed magnetic response.

magnetorheological (MR) effect characterized by an enhanced stiffness (G') and a decrease of damping $(\tan \delta)$ as the magnetic field was continuously enhanced from 0 to 1 T (Figure 4c,d). The storage modulus G' of the MATEs exhibits an S-shape with elevated magnetic field and equilibrating at 1 T. Magnetization of the particles enhances their magnetic interactions resulting in particle rearrangement, which in turn leads to an increase in the elastic modulus. It is also noted that the loss modulus G'' increases with magnetic field strength, presumably due to enhancement of friction in the course of

structuring of MPs. Nevertheless, the elastic contribution dominates, resulting in a reduction of the damping factor as the field increases.

The MR effect can be quantified as MRE = $\Delta G'/G_0'$, where $\Delta G'$ is the difference between the storage modulus measured at the oscillation frequency 10 rad/s at B=0 T and at B=1 T (G_0' and G_{\max}' respectively). An additional characteristic, $\Delta \tan \delta/\tan \delta(B=0)$, can be introduced for the damping factor. The values of $\Delta G'/G_0'$ and $\Delta \tan \delta/\tan \delta(B=0)$ for all MATEs are summarized in Table 2, which reveals that the $\Delta G'$ and $|\Delta \tan \delta|$

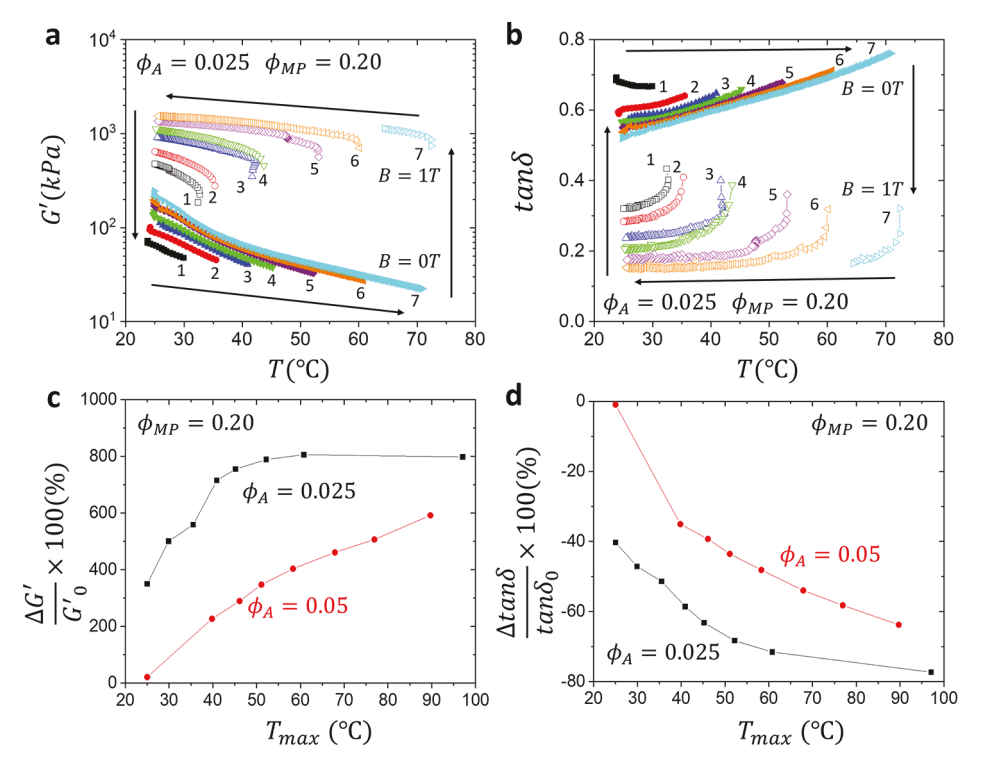


Figure 6. Programming the MR effect in MATEs. (a) Storage modulus and (b) tan δ in cycles of heating and cooling with increasing maximum annealing temperature T_{max} . Cycle numbers are noted next to the prospective curves and correspond to different T_{max} values, where 1 T field was switched on. The relative change of (c) storage modulus and (d) tan δ of the MATE depending on T_{max} for matrices with different volume fractions of PS-blocks containing 20 vol % of MPs ($\phi_{\text{MP}} = 0.20$).

 δ l grow considerably with $\phi_{\rm MP}$. The effect is particularly strong for the soft matrix ($\phi_{\rm A}=0.025$). The stiffer MATEs ($\phi_{\rm A}=0.05$) exhibit a less pronounced MR effect due to higher elastic forces which hinder MP rearrangement in the magnetic field. In general, the MR effect of MATEs is less than that observed with chemically cross-linked MAEs based on both linear strands and molecular bottlebrushes due to the higher initial modulus of the former. ^{19,28}

Programming Structure and Viscoelastic Properties of MATEs by Magnetic Field and Temperature. The thermally sensitive nature of the A-g-B matrix can be used to tune the magnetic response of the MATEs by programming the structures formed by MPs in situ. As an example, Figure 5a,b shows the change of the storage modulus and the damping factor, respectively, of MATE 2.5-CI-20 in a heating cycle with subsequent cooling in a magnetic field. Heating of the sample (point 1) with an isotropic distribution of MPs above the melting temperature (tan $\delta > 1$, point 2) releases MPs, which can then rearrange in the magnetic field, where the material dramatically stiffens (transition from point 2 to point 3), as happens in magnetic fluids. 41 The increase of G' upon application of the magnetic field of 1 T exceeds 2 orders of magnitude. Simultaneously, the damping factor drops indicating a significant enhancement in elasticity. Note that G' and $\tan \delta$ measured at high T correspond to a virtual network due to interaction of magnetized MPs. Subsequent cooling of the sample in the constant magnetic field to RT results in a gradual increase of G' due to microphase separation in the A-g-B matrix and the formation of physical network. The chain-like aggregates of MPs formed at an enhanced temperature become quenched in the matrix, and the modulus of the final anisotropic sample at zero field is higher than that of the initial sample. A portion of the drop in G' when the magnetic

field is turned off (transition from point 4 to point 5) is explained by the demagnetization of MPs. Alignment of the magnetic filler particles after quenching in the magnetic field is observed by electron microscopy (Figure 5c). Cyclic treatment following the aforementioned process demonstrates good reproducibility of results (Figure S3). The prepared anisotropic MATEs promptly respond to on—off 1 T field alterations while maintaining its newly programmed magnetic response (Figure 5d)

Thermo-magnetic processing of an isotropic MATE makes it possible to transform the isotropic material into an anisotropic composite with distinct viscoelastic properties. The induced anisotropy manifests itself in an increase in the elastic modulus and a decrease in tan δ , where the relative change of the modulus and damping factor grows with $\phi_{\rm MP}$ (Table 2). This result is consistent with the corresponding behavior of chemically cross-linked MAEs. In contrast to covalently cross-linked MAEs where particle distribution is set post-cure, MATEs allow particle rearrangement by applying a magnetic field at elevated temperatures. Furthermore, the induced anisotropy of particle distribution considerably enhances the MR effect with modulus growth several times higher in the magnetic field of 1 T than that of the initial isotropic MATEs.

Cyclic Treatment of MATEs by Temperature and Magnetic Field. Controlling the maximum heating temperature of heating—cooling cycles in the magnetic field allows tuning the viscoelastic properties and magnetic response of MATEs in a wide range as a result of the induced magnetic structure. Figure 6a,b shows temperature dependence of the storage modulus and the damping factor for heating—cooling cycles with gradually increasing temperature for the sample 2.5-CI-20 (the corresponding dependences for the other compositions are shown in Figure S4). The cooling is

performed in the magnetic field of 1 T. The main stages of the process are as follows. (i) Heating of the sample in the absence of any magnetic field from RT of 25 °C until a maximum treatment temperature $T_{\rm max}$. The value of $T_{\rm max}$ is the lowest in the first cycle (30 °C) and gradually increases in each cycle up to 72 °C. Note that this polymer matrix has $T_{\rm flow} = 57$ °C. Upon heating, the matrix becomes more compliant, as evidenced by G' decrease (filled symbols in Figure 6a,b). (ii) At each $T_{\rm max}$, the magnetic field of 1 T is switched on followed by cooling the sample to 25 °C. The field application results in significant modulus increase and correspondingly damping decrease (empty symbols in Figure 6a,b). When the temperature reaches 25 °C, the magnetic field is turned off, and the next stage of heating with an increased $T_{\rm max}$ starts at zero field.

After each cycle, the newly arranged particles within the A-g-B matrix produce different viscoelastic properties and magnetic field responses. The dependence of the MR effect in MATE *x*-CI-20 on the maximum treatment temperature T_{max} is demonstrated in Figure 6c,d. Due to the physical nature of the network formed by segregating A-g-B copolymers, some rearrangement of the magnetic filler can occur even below the melting temperature of the composite. The extent of this rearrangement increases with $T_{\rm max}$ resulting in an enhanced MR effect. The maximum MR effect is reached after sample treatment above flow temperature T_{flow} , where particles experience least steric hindrance from the matrix. It should be noted that the aggregates of MPs formed under the influence of the magnetic field appear to be quite stable as the oriented structures remain in the samples for at least 1 month, as confirmed by electron microscopy (Figure 5c).

CONCLUSIONS

In this paper, we present an innovative platform for the development of magnetically active polymeric materials with programmable mechanical properties and magnetic response. It is based on a thermally active A-g-B brush copolymer matrix with embedded magnetic microparticles, representing a distinct class of MATEs. At RT, the developed MATEs exhibit the magneto-responsive properties typical of conventional MAEs. However, they benefit from bottlebrush architecture of the network strands providing tissue-mimetic softness for magnetic response, strain-stiffening for strength, as well as solvent-free molding for MATE fabrication. The combination of the architectural control of the A-g-B copolymers with the magnetic properties of the filler particles makes it possible to vary the elastic modulus and damping over a wide range, achieving high values of the MR effect without addition of lowmolecular-mass plasticizers.

The thermal activity of the A-g-B matrix brings a valuable quality to the material and gives us the most attractive tool to program in situ the properties of MATEs. Heating makes the matrix more compliant and increases the degree of translational and rotational freedom of MPs, which can then restructure under applied magnetic field. Altered arrangements of particles created at elevated temperature can be fixed when the material is cooled in a magnetic field. Varying the value of the treatment temperature and the magnetic field, one can control the structures of MPs and, thus, the magnetic response of the MATEs in a wide range. The highest level of particle restructuring is achieved above the melting temperature of the matrix, and it allowed us to transform initially isotropic material into anisotropic one with an almost three-fold increase

in elastic modulus and up to 7.5× enhancement of the MR effect

The focus of this research was on viscoelastic properties of MATEs but it should be mentioned that the developed platform obviously allows one to alter any physical property of MATEs that depends on the arrangement of MPs. In addition, MATE activity in combined magnetic field-temperature coordinates allows reprogramming of the MATE shape and internal alignment of MPs through controlled reconfiguration of the external magnetic field (for instance, applying magnetic fields of various orientations), which gives broader operation scenarios, thereby increasing their practical importance for biomedicine and soft robotics in comparison with conventional MAEs.

METHODS

Uniaxial Tensile Tests. Dog bone-shaped samples with bridge dimensions of 12 mm \times 2 mm \times 1 mm were loaded to a RSA-G2 DMA (TA Instruments), subjected to uniaxial elongation at 22 °C, and a constant strain rate of 0.005 s⁻¹. For each sample, tests were conducted at least three times to ensure reproducibility and standard error of the elastic modulus within 5%.

Rheology. Frequency sweeps of the samples were performed on an ARES-G2 Rheometer (TA Instruments) at 5% strain using the 8 mm disk geometry in the absence of a magnetic field. Storage (G')and loss (G") modulus (and tan δ) were measured from 10^{-2} to 10^{2} Hz at RT (22 °C). To determine the flow temperature, G' and G''(and tan δ) were measured at 1 Hz from 25 to 200 °C (strain = 5%). The flow temperature was determined as the temperature where G'surpassed G' (tan $\delta = 1$). Rheological studies for comparison of viscoelasticity in and out of a magnetic field were performed using a commercial rheometer (Anton Paar, model Physica MCR 302) with the measuring unit of the plate-plate geometry and the magnetic cell MR MRD 170/1 T. Measurements of the dynamic modulus were carried out in the dynamic mode of forced torsion oscillations. Disklike samples with the diameter of 20 mm were fixed between the immobile lower plate of the measuring unit and the upper measuring head that was connected to the rotor and performed harmonic oscillations with the shear strain $\gamma = \gamma_0 \sin(\omega t)$ where γ_0 is a shear strain amplitude and ω is the angular frequency. All measurements were carried out in the linear viscoelastic regime at the shear strain amplitude equal to γ_0 = 0.001. For frequency tests, the angular frequency was varied in the range $\omega = 1-100$ rad/s. When sweeping in temperature and magnetic field, the angular frequency was fixed at 10 rad/s. In the heating—cooling cycles, the temperature varied from

A magnetic field produced in the magnetic cell by an electromagnet was oriented perpendicular to the measuring plate. The magnetic flux density B was controlled by the driving current and was varied between 0 and 1 T.

ASSOCIATED CONTENT

Supporting Information

The Supporting Information is available free of charge at https://pubs.acs.org/doi/10.1021/acsapm.3c01334.

Synthesis and molecular characterization of A-g-B bottlebrush graft copolymers, method description, and temperature dependence of MATE modulus for different volume fractions of MPs (PDF)

AUTHOR INFORMATION

Corresponding Authors

Sergei S. Sheiko — Department of Chemistry, University of North Carolina at Chapel Hill, Chapel Hill, North Carolina 27599, United States; orcid.org/0000-0003-3672-1611; Email: sergei@email.unc.edu

Elena Yu. Kramarenko — Faculty of Physics, Lomonosov Moscow State University, Moscow 119991, Russian Federation; oorcid.org/0000-0003-1716-7010; Email: kram@polly.phys.msu.ru

Authors

Sergei A. Kostrov — Faculty of Physics, Lomonosov Moscow State University, Moscow 119991, Russian Federation Mitchell R. Maw — Department of Chemistry, University of North Carolina at Chapel Hill, Chapel Hill, North Carolina 27599, United States; orcid.org/0000-0002-1921-4266

Complete contact information is available at: https://pubs.acs.org/10.1021/acsapm.3c01334

Author Contributions

S.A.K. conducted dynamic mechanical tests in the magnetic field and analyzed the obtained data; M.M. designed, synthesized, and characterized the macromonomers and polymer networks; and E.Y.K. and S.S.S were primary writers of the manuscript. All authors discussed the results and provided feedback on the manuscript.

Notes

The authors declare no competing financial interest.

ACKNOWLEDGMENTS

This work (design of MATEs, dynamic mechanical tests, and data analysis) was financially supported by the Russian Science Foundation (grant no. 19-13-00340-II). Access to electronic scientific resources was provided by the Lomonosov Moscow State University. SEM investigation of MATEs was made using the equipment of the Collaborative Access Center "Center for Polymer Research" of ISPM RAS. S.A.K. is grateful to the Theoretical Physics and Mathematics Advancement Foundation BASIS for financial support. S.S.S. and M.M. (MATE synthesis and characterization) acknowledge funding from the National Science Foundation (DMR 1921835 and DMR 2004048).

REFERENCES

- (1) Fuhrer, R.; Schumacher, C. M.; Zeltner, M.; Stark, W. J. Soft Iron/Silicon Composite Tubes for Magnetic Peristaltic Pumping: Frequency-Dependent Pressure and Volume Flow. *Adv. Funct. Mater.* **2013**, 23, 3845–3849.
- (2) Zhao, X.; Kim, J.; Cezar, C. A.; Huebsch, N.; Lee, K.; Bouhadir, K.; Mooney, D. J. Active Scaffolds for On-Demand Drug and Cell Delivery. *Proc. Natl. Acad. Sci. U.S.A.* **2011**, *108*, 67–72.
- (3) Nguyen, V. Q.; Ahmed, A. S.; Ramanujan, R. V. Morphing Soft Magnetic Composites. *Adv. Mater.* **2012**, *24*, 4041–4054.
- (4) Alekhina, I.; Kramarenko, E.; Makarova, L.; Perov, N. Magnetorheological Composites for Biomedical Applications. In *Magnetic Materials and Technologies for Medical Applications*; Tishin, A. M., Ed.; Woodhead Publishing Series in Electronic and Optical Materials; Woodhead Publishing, 2022; pp 501–526.
- (5) Li, Y.; Li, J.; Li, W.; Du, H. A State-of-the-Art Review on Magnetorheological Elastomer Devices. *Smart Mater. Struct.* **2014**, 23, 123001.
- (6) Kramarenko, E. Yu.; Stepanov, G. V.; Stepanov, A. R.; Khokhlov, A. R. Magnetically Active Silicone Elastomers: Twenty Years of Development. *INEOS Open* **2020**, *2*, 178–184.
- (7) Shamonin, M.; Kramarenko, E. Y. Highly Responsive Magnetoactive Elastomers. In *Novel Magnetic Nanostructures. Unique Properties and Applications*, 1st ed.; Domracheva, N.; Caporali, M.; Rentschler, E., Eds.; Elsevier: Amsterdam, Netherlands, 2018; pp 221–245.

- (8) Ubaidillah; Sutrisno, J.; Purwanto, A.; Mazlan, S. A. Recent Progress on Magnetorheological Solids: Materials, Fabrication, Testing, and Applications. *Adv. Eng. Mater.* **2015**, *17*, 563–597.
- (9) Bastola, A. K.; Paudel, M.; Li, L.; Li, W. Recent Progress of Magnetorheological Elastomers: A Review. *Smart Mater. Struct.* **2020**, 29, 123002.
- (10) Nadzharyan, T. A.; Shamonin, M.; Kramarenko, E. Y. Theoretical Modeling of Magnetoactive Elastomers on Different Scales: A State-of-the-Art Review. *Polymers* **2022**, *14*, 4096.
- (11) Menzel, A. M. Tuned, Driven, and Active Soft Matter. *Phys. Rep.* **2015**, *554*, 1–45.
- (12) Filipcsei, G.; Csetneki, I.; Szilágyi, A.; Zrínyi, M. Magnetic Field-Responsive Smart Polymer Composites. In *Oligomers-Polymer Composites-Molecular Imprinting*; Gong, B., Sanford, A. R., Ferguson, J. S., Eds.; Advances in Polymer Science; Springer: Berlin, Heidelberg, 2007; pp 137–189.
- (13) Odenbach, S. Microstructure and Rheology of Magnetic Hybrid Materials. *Arch. Appl. Mech.* **2016**, *86*, 269–279.
- (14) Rubinstein, M.; Colby, R. H. *Polymer Physics*, 1st ed.; Oxford University Press, 2003; Section 7.3, pp 264–268.
- (15) Schmauch, M. M.; Mishra, S. R.; Evans, B. A.; Velev, O. D.; Tracy, J. B. Chained Iron Microparticles for Directionally Controlled Actuation of Soft Robots. *ACS Appl. Mater. Interfaces* **2017**, *9*, 11895—11901.
- (16) Ding, L.; Zhang, J.; Shu, Q.; Liu, S.; Xuan, S.; Gong, X.; Zhang, D. Magnetism-Responsive Anisotropic Film with Self-Sensing and Multifunctional Shape Manipulation. *ACS Appl. Mater. Interfaces* **2021**, *13*, 13724–13734.
- (17) Abramchuk, S.; Kramarenko, E.; Stepanov, G.; Nikitin, L. V.; Filipcsei, G.; Khokhlov, A. R.; Zrínyi, M. Novel Highly Elastic Magnetic Materials for Dampers and Seals: Part I. Preparation and Characterization of the Elastic Materials. *Polym. Adv. Technol.* **2007**, *18*, 883–890.
- (18) Abramchuk, S.; Kramarenko, E.; Grishin, D.; Stepanov, G.; Nikitin, L. V.; Filipcsei, G.; Khokhlov, A. R.; Zrínyi, M. Novel Highly Elastic Magnetic Materials for Dampers and Seals: Part II. Material Behavior in a Magnetic Field. *Polym. Adv. Technol.* **2007**, *18*, 513–518.
- (19) Sorokin, V. V.; Ecker, E.; Stepanov, G. V.; Shamonin, M.; Monkman, G. J.; Kramarenko, E. Y.; Khokhlov, A. R. Experimental Study of the Magnetic Field Enhanced Payne Effect in Magnetorheological Elastomers. *Soft Matter* **2014**, *10*, 8765–8776.
- (20) Stepanov, G. V.; Abramchuk, S. S.; Grishin, D. A.; Nikitin, L. V.; Kramarenko, E. Yu.; Khokhlov, A. R. Effect of a Homogeneous Magnetic Field on the Viscoelastic Behavior of Magnetic Elastomers. *Polymer* **2007**, *48*, 488–495.
- (21) Romeis, D.; Toshchevikov, V.; Saphiannikova, M. Elongated Micro-Structures in Magneto-Sensitive Elastomers: A Dipolar Mean Field Model. *Soft Matter* **2016**, *12*, 9364–9376.
- (22) Ivaneyko, D.; Toshchevikov, V.; Saphiannikova, M. Dynamic-Mechanical Behaviour of Anisotropic Magneto-Sensitive Elastomers. *Polymer* **2018**, *147*, 95–107.
- (23) Farshad, M.; Benine, A. Magnetoactive Elastomer Composites. *Polym. Test.* **2004**, 23, 347–353.
- (24) Puente-Córdova, J.; Reyes-Melo, M. E.; Palacios-Pineda, L. M.; Martínez-Perales, I. A.; Martínez-Romero, O.; Elías-Zúñiga, A. Fabrication and Characterization of Isotropic and Anisotropic Magnetorheological Elastomers, Based on Silicone Rubber and Carbonyl Iron Microparticles. *Polymers* **2018**, *10*, 1343.
- (25) Lin, D.; Yang, F.; Gong, D.; Lin, Z.; Li, R.; Qian, W.; Li, C.; Jia, S.; Chen, H. Magnetoactive Soft Drivers with Radial-Chain Iron Microparticles. ACS Appl. Mater. Interfaces 2021, 13, 34935—34941.
- (26) Lu, H.; Zhang, M.; Yang, Y.; Huang, Q.; Fukuda, T.; Wang, Z.; Shen, Y. A Bioinspired Multilegged Soft Millirobot That Functions in Both Dry and Wet Conditions. *Nat. Commun.* **2018**, *9*, 3944.
- (27) Dashtimoghadam, E.; Maw, M.; Keith, A. N.; Vashahi, F.; Kempkes, V.; Gordievskaya, Y. D.; Kramarenko, E. Y.; Bersenev, E. A.; Nikitina, E. A.; Ivanov, D. A.; Tian, Y.; Dobrynin, A. V.; Vatankhah-Varnosfaderani, M.; Sheiko, S. S. Super-Soft, Firm, and Strong

- Elastomers toward Replication of Tissue Viscoelastic Response. *Mater. Horiz.* **2022**, *9*, 3022–3030.
- (28) Kostrov, S. A.; Dashtimoghadam, E.; Keith, A. N.; Sheiko, S. S.; Kramarenko, E. Yu. Regulating Tissue-Mimetic Mechanical Properties of Bottlebrush Elastomers by Magnetic Field. *ACS Appl. Mater. Interfaces* **2021**, *13*, 38783–38791.
- (29) Maw, M.; Morgan, B. J.; Dashtimoghadam, E.; Tian, Y.; Bersenev, E. A.; Maryasevskaya, A. V.; Ivanov, D. A.; Matyjaszewski, K.; Dobrynin, A. V.; Sheiko, S. S. Brush Architecture and Network Elasticity: Path to the Design of Mechanically Diverse Elastomers. *Macromolecules* **2022**, *55*, 2940–2951.
- (30) Maw, M.; Dashtimoghadam, E.; Keith, A. N.; Morgan, B. J.; Tanas, A. K.; Nikitina, E.; Ivanov, D. A.; Vatankhah-Varnosfaderani, M.; Dobrynin, A. V.; Sheiko, S. S. Sticky Architecture: Encoding Pressure Sensitive Adhesion in Polymer Networks. *ACS Cent. Sci.* 2023, *9*, 197–205.
- (31) Semisalova, A. S.; Perov, N. S.; Stepanov, G. V.; Kramarenko, E. Y.; Khokhlov, A. R. Strong Magnetodielectric Effects in Magnetorheological Elastomers. *Soft Matter* **2013**, *9*, 11318–11324.
- (32) Depalle, B.; Qin, Z.; Shefelbine, S. J.; Buehler, M. J. Influence of Cross-Link Structure, Density and Mechanical Properties in the Mesoscale Deformation Mechanisms of Collagen Fibrils. *J. Mech. Behav. Biomed. Mater.* **2015**, 52, 1–13.
- (33) Daniel, W. F. M.; Burdyńska, J.; Vatankhah-Varnoosfaderani, M.; Matyjaszewski, K.; Paturej, J.; Rubinstein, M.; Dobrynin, A. V.; Sheiko, S. S. Solvent-Free, Supersoft and Superelastic Bottlebrush Melts and Networks. *Nat. Mater.* **2016**, *15*, 183–189.
- (34) Vatankhah-Varnosfaderani, M.; Daniel, W. F. M.; Everhart, M. H.; Pandya, A. A.; Liang, H.; Matyjaszewski, K.; Dobrynin, A. V.; Sheiko, S. S. Mimicking Biological Stress-Strain Behaviour with Synthetic Elastomers. *Nature* **2017**, *549*, 497–501.
- (35) Vatankhah-Varnosfaderani, M.; Keith, A. N.; Cong, Y.; Liang, H.; Rosenthal, M.; Sztucki, M.; Clair, C.; Magonov, S.; Ivanov, D. A.; Dobrynin, A. V.; Sheiko, S. S. Chameleon-like Elastomers with Molecularly Encoded Strain-Adaptive Stiffening and Coloration. *Science* 2018, 359, 1509–1513.
- (36) Dobrynin, A. V.; Carrillo, J.-M. Y. Universality in Nonlinear Elasticity of Biological and Polymeric Networks and Gels. *Macromolecules* **2011**, *44*, 140–146.
- (37) Kuthe, C. D.; Uddanwadiker, R. V. Investigation of Effect of Fiber Orientation on Mechanical Behavior of Skeletal Muscle. *J. Appl. Biomater. Funct. Mater.* **2016**, *14*, e154–162.
- (38) Keith, A. N.; Vatankhah-Varnosfaderani, M.; Clair, C.; Fahimipour, F.; Dashtimoghadam, E.; Lallam, A.; Sztucki, M.; Ivanov, D. A.; Liang, H.; Dobrynin, A. V.; Sheiko, S. S. Bottlebrush Bridge between Soft Gels and Firm Tissues. *ACS Cent. Sci.* **2020**, *6*, 413–419.
- (39) Holzapfel, G. A.; Sommer, G.; Gasser, C. T.; Regitnig, P. Determination of Layer-Specific Mechanical Properties of Human Coronary Arteries with Nonatherosclerotic Intimal Thickening and Related Constitutive Modeling. *Am. J. Physiol. Heart Circ. Physiol.* 2005, 289, H2048–H2058.
- (40) Silver, F. H.; Snowhill, P. B.; Foran, D. J. Mechanical Behavior of Vessel Wall: A Comparative Study of Aorta, Vena Cava, and Carotid Artery. *Ann. Biomed. Eng.* **2003**, *31*, 793–803.
- (41) de Vicente, J.; Klingenberg, J.; Hidalgo-Alvarez, R. Magneto-rheological Fluids: A Review. *Soft Matter* **2011**, *7*, 3701–3710.